AIAA JOURNAL
Vol. 43, No. 4, April 2005

Acoustic Source Terms for the Linearized Euler Equations in Conservative Form

Mattias Billson,* Lars-Erik Eriksson,† and Lars Davidson†
Chalmers University of Technology, SE-412 96 Göteborg, Sweden

A rather novel approach to predict jet noise is the stochastic noise generation and radiation (SNGR) method. The SNGR method uses the linearized Euler equations as an acoustic analogy together with source terms that are modeled. Previously, source terms for the linearized Euler equations have been derived and presented by Goldstein (Goldstein, M. E., "A Unified Approach to Some Recent Developments in Jet Noise Theory," *International Journal of Aeroacoustics*, Vol. 1, No. 1, 2002, pp. 1–16), as well as Bailly et al. (Bailly, C., Lafon, P., and Candel, S. M., "A Stochastic Approach to Compute Noise Generation and Radiation of Free Turbulent Flows," AIAA Paper 95-092, June 1995). Two different nonconservative formulations of the inhomogeneous linearized Euler equations are presented in these previous studies. Because the linearized Euler equations in conservative form are used in the present work, new source terms have to be derived for the conservative set of equations. A formal derivation of source terms for the linearized Euler equations in conservative form is presented, and the system of equations is compared to those of Goldstein and Bailly et al. Simplified versions of the derived source terms are also developed. To test the derived source terms, a direct simulation of a forced two-dimensional mixing layer is carried out. The direct simulation provides the mean flow and source field for the inhomogeneous linearized Euler equations. The solutions to the linearized Euler equations with source terms are compared to the solution of the direct simulation and show good agreement. All simulations are performed using Tam and Webb's fourth-order dispersion-relation-preserving scheme and a four-step fourth-order Runge–Kutta time-marching technique. Artificial selective damping introduced through the numerical scheme is used to avoid spurious waves. Absorbing boundary conditions based on characteristic variables are used at the free boundaries and a buffer layer is added at the outflow.

Nomenclature

A	=	inflow forcing strength
a_i, c_i, d_i	=	numerical coefficients
C_p	=	specific heat at constant pressure $(\partial h/\partial T)_p$
c	=	speed of sound
e	=	energy per unit mass
f_0	=	forcing frequency
h	=	enthalpy per unit mass
M	=	Mach number
p	=	pressure
$\boldsymbol{Q}$	=	conservative variables solution vector
$\mathcal{Q}$	=	heat source term
T	=	temperature, period time
$\mathcal{T}$	=	Reynolds stress source term
t	=	time
U	=	mean x velocity
u, v, w	=	x, y, z velocities
x, y, z	=	spatial coordinates
$x_0, x_{\max}$	=	buffer-layer limits
α	=	timescale parameter
γ	=	specific heat ratio
Δ	=	grid spacing
δ_{ij}	=	Kronecker delta
$\delta_\omega(0)$	=	initial shear layer thickness
ϵ	=	upwinding parameter
Θ	=	dilatation, $\partial u_i/\partial x_i$
λ	=	acoustic wavelength
ν	=	kinematic molecular viscosity
ρ	=	density
$\sigma_{\max}$	=	maximum buffer-layer strength
$\sigma(x, y)$	=	buffer-layer strength function
φ	=	angle from x direction
ω_0	=	forcing angular frequency

Subscripts

i, j, k	=	indices
in	=	inflow condition
(n)	=	time step number
p	=	pairing
0	=	ambient, total or inflection point

Superscripts

$\bar{\cdot}$	=	time average
$\tilde{\cdot}$	=	Favre time average
$\hat{\cdot}$	=	defined reference variable
$'$	=	time-average associated fluctuation
$''$	=	Favre-average associated fluctuation
$'''$	=	fluctuation associated to $\hat{\cdot}$
$*$	=	low-pass filtered value

Received 30 September 2002; accepted for publication 27 July 2004.

*Assistant Professor, Division of Thermo and Fluid Dynamics.
†Professor, Division of Thermo and Fluid Dynamics.

Introduction

USING acoustic analogies to retrieve acoustic information from a source field is a computationally efficient way to compute the far-field noise of a turbulent flow. There are a variety of analogies which can be used, Lighthill's[1] analogy for free turbulence in a homogeneous medium at rest, Lilley's[2] analogy to account for refraction, and Curle's[3] extension to Lighthill's analogy for the presence of solid walls just to mention a few.

Lighthill's analogy is most often solved in integral form and limited by the assumption of sound generation and radiation in a homogeneous medium at rest. Because the wave operator does not govern refractional effects, these must be completely specified by the source field used to evaluate the source terms. The same limitations holds for Curle's extension to Lighthill's analogy. Although the wave operator in Lilley's analogy does include refractional effects, it is somewhat sensitive to the way the source terms are evaluated (see Ref. 4). The linearized Euler equations with source terms are not limited by the homogeneous medium assumption and can

handle refractional effects and reflection at solid boundaries. The scalar wave equation in Lighthill's analogy governs acoustic wave propagation but not entropy and vorticity waves. The linearized Euler equations, on the other hand, govern both acoustic propagation and entropy and vorticity waves, allowing interaction between the different wave forms.

This work is part an evaluation and development of the stochastic noise generation and radiation (SNGR) method originally presented by Bechara et al.[5] and further developed by Bailly et al.[6] and Bailly and Juvé.[7] Modified versions of the SNGR method have also been presented by Billson et al.[8–10]

The present paper focuses on the formulation of source terms for the linearized Euler equations. In Ref. 6, a formulation of the linearized Euler equations based on $(\rho', \bar{\rho}u', \bar{\rho}v', \bar{\rho}w', p')$ as solution variables is used. In that formulation, because pressure rather than energy is solved for, the source terms only enter the momentum equations. Goldstein[11] presented a formulation of the linearized Euler equations with source terms based on $[\rho', \rho u'', \rho v'', \rho w'', (\rho e)']$. In this formulation, source terms enter the momentum and energy equations. Both formulations of the linearized Euler equations are nonconservative formulations in terms of conservation of mass, momentum, and energy. If the reference (mean) solution is obtained with a solver based on a conservative formulation of the flow equations, it is advantageous to use the conservative formulation of the linearized Euler equations as well. The risk of spurious disturbances in the solution to the linearized Euler equations is then minimized. The formulation of the linearized Euler equations used in the present work is based on conservative variables $[\rho', (\rho u)', (\rho v)', (\rho w)', (\rho e_0)']$. In this formulation, the source terms enter the momentum equations and the equation for the total energy. A proposed formulation of source terms for the linearized Euler equations in conservative form will be derived. This set of equations is then compared to those in Refs. 6 and 11. In the present formulation, the source terms do not only depend on the unsteady Reynolds stresses but also on unsteady total enthalpy. This causes some problems in the SNGR method. In the formulations of the SNGR method,[5–8] only velocity fluctuations are modeled in the source terms, assuming that all other variables are constant. For this reason, different simplifications of the source terms are derived in the present study.

The use of a forced two-dimensional mixing layer as a test case for different acoustic analogies was first presented by Colonius et al.,[4] who performed a direct numerical simulation (DNS) of a free mixing layer forced at its first three harmonics. The results were used and compared with Lilley's acoustic analogy.[2] Later Bogey et al.[12,13] made a sound prediction with large eddy simulation (LES) and Lighthill's analogy, as well as LES and the linearized Euler equations (as derived in Ref. 6) on a free mixing layer excited by the first two harmonics. The results in the preceding cases were in good agreement between the direct simulations and the analogies. To test the derived source terms in the present formulation of linearized Euler equations, a forced mixing layer is computed by direct simulation using a two-dimensional compressible Navier–Stokes solver. The solution from the direct simulation provides a reference solution (time average) and is used to evaluate the source terms for the linearized Euler equations, which are solved and the results are compared. Comparisons of the computational results using the different source terms with the direct simulation of a forced free mixing layer are presented and discussed.

Theory

In this section, a derivation of the linearized Euler equations and energy equation in conservative form with source terms is presented. The derivation starts with the Euler equations and is a rewriting of the full Euler equations in a way that the left-hand side of the equations are the linearized Euler equations. The remaining nonlinear terms in this derivation are put in the right-hand side and form the source terms.

Start with the compressible Euler equations in conservative form:

$$\frac{\partial \rho}{\partial t} + \frac{\partial \rho u_j}{\partial x_j} = 0 \tag{1}$$

$$\frac{\partial \rho u_i}{\partial t} + \frac{\partial}{\partial x_j}(\rho u_i u_j + p\delta_{ij}) = 0 \tag{2}$$

$$\frac{\partial \rho e_0}{\partial t} + \frac{\partial}{\partial x_j}(\rho h_0 u_j) = 0 \tag{3}$$

where $(\rho, \rho u, \rho v, \rho w, \rho e_0)$ are the density; the x, y and z momentum; and the total energy per unit volume. Together with an equation of state, this forms a closed set of equations. If it is assumed that the fluid behaves as an ideal gas with constant specific heats, the pressure and total enthalpy per unit volume ρh_0 are related to the solution variables as

$$p = (\gamma - 1)\left[\rho e_0 - \tfrac{1}{2}(\rho u_k)(\rho u_k)/\rho\right], \qquad \rho h_0 = \rho e_0 + p \tag{4}$$

and they are introduced to allow for a more compact notation. A decomposition of the variables in a time-averaged part and a fluctuating part is denoted as

$$\rho = \bar{\rho} + \rho', \qquad u_i = \tilde{u}_i + u_i'', \qquad e_0 = \tilde{e}_0 + e_0''$$
$$p = \bar{p} + p', \qquad h_0 = \tilde{h}_0 + h_0'' \tag{5}$$

where bar and prime denote time-average and associated fluctuation, respectively. A tilde denotes Favre average and is, for u_i, for example, defined by

$$\tilde{u}_i = \overline{\rho u_i}/\bar{\rho} \tag{6}$$

and the double prime is the fluctuation associated with the Favre time average. The decompositions of total enthalpy and pressure are consistent with the decompositions of the primary solution variables $(\rho, \rho u, \rho v, \rho w, \rho e_0)$, and the total enthalpy will be retained in the following derivation to simplify the notation of the energy equation.

To prepare for the decomposition of the equations into an average part and a fluctuation, a few identities will be derived. First, the momentum can be decomposed in two ways:

$$\rho u_i = \overline{\rho u_i} + (\rho u_i)' = \bar{\rho}\tilde{u}_i + (\rho u_i)' \tag{7a}$$

or

$$\rho u_i = \rho(\tilde{u}_i + u_i'') = \rho\tilde{u}_i + \rho u_i'' \tag{7b}$$

which implies that

$$(\rho u_i)' = \rho'\tilde{u}_i + \rho u_i'' \tag{8}$$

The first decomposition in Eq. (7) is done by time averaging ρu_i and the second by Favre averaging u_i. Similarly, we obtain

$$(\rho e_0)' = \rho'\tilde{e}_0 + \rho e_0'', \qquad (\rho h_0)' = \rho'\tilde{h}_0 + \rho h_0'' \tag{9}$$

Second,

$$\rho h_0 u_j = \rho(\tilde{h}_0 + h_0'')(\tilde{u}_j + u_j'')$$
$$= \rho\tilde{h}_0\tilde{u}_j + \rho\tilde{h}_0 u_j'' + \rho h_0''\tilde{u}_j + \rho h_0'' u_j'' \tag{10}$$

which implies that

$$\overline{\rho h_0 u_j} = \bar{\rho}\tilde{h}_0\tilde{u}_j + \overline{\rho h_0'' u_j''} \tag{11}$$

Equations (4–11) will be used to rewrite Eqs. (1–3) into the linearized Euler equations with source terms. Taking the time-average of the continuity equation (1) gives

$$\frac{\partial \bar{\rho}}{\partial t} + \frac{\partial \overline{\rho u_j}}{\partial x_j} = 0 \tag{12}$$

Subtraction of Eq. (12) from Eq. (1) results in the continuity equation for the fluctuations:

$$\frac{\partial \rho'}{\partial t} + \frac{\partial (\rho u_j)'}{\partial x_j} = 0 \tag{13}$$

Inserting the decomposition in Eq. (5) into the momentum equation (2) and time averaging gives

$$\frac{\partial \bar{\rho}\tilde{u}_i}{\partial t} + \frac{\partial}{\partial x_j}(\bar{\rho}\tilde{u}_i\tilde{u}_j + \overline{\rho u_i'' u_j''} + \bar{p}\delta_{ij}) = 0 \tag{14}$$

Subtracting the resulting Eq. (14) from Eq. (2) gives an equation for the fluctuations:

$$\frac{\partial \rho u_i - \bar{\rho}\tilde{u}_i}{\partial t} + \frac{\partial}{\partial x_j}(\rho u_i u_j - \bar{\rho}\tilde{u}_i\tilde{u}_j - \overline{\rho u_i'' u_j''} + (p-\bar{p})\delta_{ij}) = 0 \tag{15}$$

Using Eq. (7) on the first term and expanding $\rho u_i u_j$ gives

$$\frac{\partial(\rho u_i)'}{\partial t} + \frac{\partial}{\partial x_j}(\rho'\tilde{u}_i\tilde{u}_j + \rho u_i''\tilde{u}_j + \rho u_j''\tilde{u}_i + \rho u_i'' u_j'' - \overline{\rho u_i'' u_j''} + p'\delta_{ij}) = 0 \tag{16}$$

Using Eq. (8) on the second term and rewriting the resulting equation by moving all nonlinear terms to the right-hand side gives

$$\frac{\partial(\rho u_i)'}{\partial t} + \frac{\partial}{\partial x_j}(\tilde{u}_j(\rho u_i)' + \tilde{u}_i(\rho u_j)' - \rho'\tilde{u}_i\tilde{u}_j + p'\delta_{ij}) = -\frac{\partial}{\partial x_j}(\rho u_i'' u_j'' - \overline{\rho u_i'' u_j''}) \tag{17}$$

Equation (17) is the linearized momentum equation on the left-hand side with source terms on the right-hand side. That the left-hand side of Eq. (17) indeed is the linearized momentum equation can be seen through differentiation of the term $\rho u_i u_j$ as

$$\begin{aligned} \mathrm{d}(\rho u_i u_j) &= \mathrm{d}[(\rho u_i)(\rho u_j)/\rho] \\ &= u_i\,\mathrm{d}(\rho u_j) + u_j\,\mathrm{d}(\rho u_i) - u_i u_j\,\mathrm{d}(\rho) \end{aligned} \tag{18}$$

and the fluctuating pressure p' in terms of the conservative variables is given by

$$p' = (\gamma - 1)\left[(\rho e_0)' - \tilde{u}_k(\rho u_k)' + \tfrac{1}{2}\tilde{u}_k\tilde{u}_k\rho'\right] \tag{19}$$

Now we proceed to derive the linearized equation for total energy. Averaging the inviscid energy equation (3) gives

$$\frac{\partial \overline{\rho e_0}}{\partial t} + \frac{\partial}{\partial x_j}(\overline{\rho h_0 u_j}) = 0 \tag{20}$$

and subtracting Eq. (20) from Eq. (3) yields

$$\frac{\partial(\rho e_0)'}{\partial t} + \frac{\partial}{\partial x_j}(\rho h_0 u_j - \overline{\rho h_0 u_j}) = 0 \tag{21}$$

Inserting expressions (10) and (11) into Eq. (21), keeping the linear terms on the left-hand side, and moving the nonlinear terms to the right-hand side gives

$$\frac{\partial(\rho e_0)'}{\partial t} + \frac{\partial}{\partial x_j}(\rho'\tilde{h}_0\tilde{u}_j + \rho\tilde{h}_0 u_j'' + \rho h_0''\tilde{u}_j) = -\frac{\partial}{\partial x_j}(\rho h_0'' u_j'' - \overline{\rho h_0'' u_j''}) \tag{22}$$

Using expressions (8) and (9), Eq. (22) can now be rewritten as

$$\frac{\partial(\rho e_0)'}{\partial t} + \frac{\partial}{\partial x_j}(\tilde{h}_0(\rho u_j)' + \tilde{u}_j(\rho h_0)' - \rho'\tilde{h}_0\tilde{u}_j) = -\frac{\partial}{\partial x_j}(\rho h_0'' u_j'' - \overline{\rho h_0'' u_j''}) \tag{23}$$

where the left-hand side is the linearized energy equation and the right-hand side contains all nonlinear terms. The resulting linearized Euler equations with source terms are summarized as

$$\begin{aligned} &\frac{\partial \rho'}{\partial t} + \frac{\partial(\rho u_j)'}{\partial x_j} = 0 \\ &\frac{\partial(\rho u_i)'}{\partial t} + \frac{\partial}{\partial x_j}(\tilde{u}_j(\rho u_i)' + \tilde{u}_i(\rho u_j)' - \rho'\tilde{u}_i\tilde{u}_j + p'\delta_{ij}) \\ &\qquad = -\frac{\partial}{\partial x_j}(\rho u_i'' u_j'' - \overline{\rho u_i'' u_j''}) \\ &\frac{\partial(\rho e_0)'}{\partial t} + \frac{\partial}{\partial x_j}(\tilde{h}_0(\rho u_j)' + \tilde{u}_j(\rho h_0)' - \rho'\tilde{h}_0\tilde{u}_j) \\ &\qquad = -\frac{\partial}{\partial x_j}(\rho h_0'' u_j'' - \overline{\rho h_0'' u_j''}) \end{aligned} \tag{24}$$

The inhomogeneous linearized Euler equations (24) have been derived from the Euler equations without approximations or assumptions of the nature of the flow. Equations (24) are in fact still the nonlinear Euler equations. However, if one argues that the terms on the right-hand side of Eqs. (24) are in some way known and considered as source terms, then the equations on the left-hand side are the linearized Euler equations. The right-hand side could, for example, be given by a large eddy simulation or a DNS, which also provides the reference solution $(\bar{\rho}, \bar{\rho}\tilde{u}, \bar{\rho}\tilde{v}, \bar{\rho}\tilde{w}, \bar{\rho}\tilde{e}_0)$ for the linearized Euler equations. Equations (24) would then be an analogy for acoustic generation and radiation.

Recently, Goldstein[11] has proposed a system of equations that is essentially the same equations as those presented in this paper [Eq. (24)] but based on the solution variables $[\rho', \rho u'', \rho v'', \rho w'', (\rho e)']$. The system of equations in Ref. 11 is given next, but the notation has been changed to fit the definitions in this paper:

$$\begin{aligned} &\frac{\partial \rho'}{\partial t} + \frac{\partial(\rho u_j)'}{\partial x_j} = 0 \\ &\frac{\partial \rho u_i''}{\partial t} + \frac{\partial}{\partial x_j}(\rho u_i''\tilde{u}_j + p'\delta_{ij}) + \rho u_j''\frac{\partial \tilde{u}_i}{\partial x_j} - \frac{\rho'}{\bar{\rho}}\frac{\partial}{\partial x_j}(\bar{p}\delta_{ij} + \overline{\rho u_i'' u_j''}) = -\frac{\partial}{\partial x_j}(\rho u_i'' u_j'' - \overline{\rho u_i'' u_j''}) \\ &\frac{\partial(\rho e)'}{\partial t} + \frac{\partial}{\partial x_j}((\rho e)'\tilde{u}_j + \rho u_j''\tilde{h}) + p'\frac{\partial \tilde{u}_j}{\partial x_j} - \frac{\rho u_i''}{\bar{\rho}}\frac{\partial}{\partial x_j}(\bar{p}\delta_{ij} + \overline{\rho u_i'' u_j''}) = -\frac{\partial}{\partial t}\left(\frac{1}{2}[\rho u_k'' u_k'' - \overline{\rho u_k'' u_k''}]\right) \\ &\qquad - \frac{\partial}{\partial x_j}\left(\tilde{u}_j\frac{1}{2}[\rho u_k'' u_k'' - \overline{\rho u_k'' u_k''}]\right) - \frac{\partial}{\partial x_j}(\rho h_0''' u_j'' - \overline{\rho h_0''' u_j''}) \\ &\qquad + \tilde{u}_j\frac{\partial}{\partial x_k}(\rho u_k'' u_j'' - \overline{\rho u_k'' u_j''}) \end{aligned} \tag{25}$$

where h_0''' is defined in Ref. 11 as

$$h_0''' = h_0 - \hat{h}_0, \qquad \hat{h}_0 = \tilde{h} + \tfrac{1}{2}\tilde{u}_k\tilde{u}_k \tag{26}$$

Equations (24) and (25) are equivalent as equations and contain the same information. They are both still the full nonlinear Euler equations but in different forms. As analogies, however, they differ in two respects.

The first is that the source terms are not the same in Eq. (24) and Eq. (25). The source terms in the momentum equations are the same, but the source terms in the energy equations differ. The source terms in Eq. (25) are quite complex and involve both time and spatial derivatives, whereas the source terms in Eq. (24) involve only spatial derivatives. Also, on the left-hand side of Eq. (25), there is a

term containing the Reynolds stress $\overline{\rho u_i'' u_j''}$, which at the same time is considered as a source term on the right-hand side.

The second difference is that the conservative formulation in Eq. (24) is numerically consistent with a Navier–Stokes solution in conservative formulation. The amount of disturbances and spurious waves generated can, thus, be kept to a minimum when the reference flowfield is consistent with the formulation of the linearized Euler equations. This is generally not the case for a nonconservative formulation such as Eq. (25). An other advantage in the conservative formulation is the possibility to introduce artificial selective damping, which is needed in the solution to the linearized Euler equations, directly through the numerical scheme. This is done by a high-order upwinding in the numerical scheme and will be briefly described. For a more thorough analysis of the artificial selective damping, see Refs. 14 and 15.

Bailly et al.[6] presented a set of linearized Euler equations with source terms to be used as an acoustic analogy that is based on $(\rho', \bar{\rho}u', \bar{\rho}v', \bar{\rho}w', p')$ as solution variables. In Ref. 6, the reference velocity variables are time-averaged variables, whereas in Eq. (24) (and in Ref. 11) the reference velocity and also the energy variables are Favre averaged. The linearized Euler equations with source terms based on $(\rho', \bar{\rho}u', \bar{\rho}v', \bar{\rho}w', p')$ as solution variables are given by

$$\frac{\partial \rho'}{\partial t} + \frac{\partial}{\partial x_j}(\bar{\rho}u_j' + \rho'\overline{u}_j) + \underline{\frac{\partial}{\partial x_j}(\rho' u_j' + \overline{\rho' u_j'})} = 0$$

$$\frac{\partial \bar{\rho}u_i'}{\partial t} + \frac{\partial}{\partial x_j}(\bar{\rho}\overline{u}_j u_i' + p'\delta_{ij}) + (\bar{\rho}u_j' + \rho'\overline{u}_j)\frac{\partial \overline{u}_i}{\partial x_j}$$
$$+ \underline{\frac{\partial \rho' u_i'}{\partial t} + \frac{\partial}{\partial x_j}(\rho' u_i'\overline{u}_j - \overline{\rho' u_i'}\overline{u}_j) + (\rho' u_j' + \overline{\rho' u_j'})\frac{\partial \overline{u}_i}{\partial x_j}}$$
$$= -\frac{\partial}{\partial x_j}(\rho u_i' u_j' - \overline{\rho u_i' u_j'})$$

$$\frac{\partial p'}{\partial t} + \frac{\partial}{\partial x_i}(p'\overline{u}_i + \gamma \bar{p}u_i') + (\gamma - 1)\left(p'\frac{\partial \overline{u}_i}{\partial x_i} - u_i'\frac{\partial \bar{p}}{\partial x_i}\right)$$
$$+ \underline{u_i'\frac{\partial p'}{\partial x_i} - \overline{u_i'\frac{\partial p'}{\partial x_i}} + \gamma\left(p'\frac{\partial u_i'}{\partial x_i} - \overline{p'\frac{\partial u_i'}{\partial x_i}}\right)} = 0 \qquad (27)$$

Equations (27) are also equivalent (as equations) to the present formulation of the inhomogeneous linearized Euler equations (24) but expressed in different solution variables. The system of equations in Ref. 6 is in part the same system of equations as Eq. (27) except that in Ref. 6 the terms in Eq. (27) that are underlined have been omitted. The omitted terms in Ref. 6 are of higher order, and the tests done with this system of equations[13] suggest that this neglect does not noticeably change the results. However, the resulting system of equations in Ref. 6 are not the same as in Ref. 11 or in the present paper [Eq. (24)].

Three formulations of the inhomogeneous linearized Euler equations have been presented. They are equivalent as equations but not as acoustic analogies because the source terms are not the same in the three formulations. They all share the minimum requirement of an acoustic analogy that the source terms should have a zero time average.

Hydrodynamic Instabilities

Unlike scalar wave operators, the linearized Euler equations also support vorticity and entropy waves. This is both an advantage and a disadvantage for the linearized Euler equations as a wave operator. The advantage is that entropy and vorticity waves generated by the source terms are indeed governed by the linearized Euler equations. The interaction of the vorticity and entropy waves with the acoustic waves may be an important factor in the sound propagation and development in inhomogeneous flows. The disadvantage is that this may cause hydrodynamic instabilities. Stability analysis of the linearized Euler equations shows that vorticity and entropy waves can grow without bound in the presence of parallel mean shear.[16] The reason for this is the absence of nonlinear terms in the linearized Euler equations. The coupling of the acoustic waves with the vorticity and entropy waves will, if the instabilities grow without bound, totally contaminate the acoustic far-field solution. If the shear flow is nonparallel, for example, diverging as in a jet or in the mixing layer used in the present work, this is in general not the case. The conditions for the instabilities vary in a diverging flow so that the unstable frequencies are not the same throughout the flowfield.

That the near-field solution is affected by the instabilities does not necessarily mean that the far-field solution is. The instabilities will not radiate much sound and contaminate the far field as long as the acoustic characteristic variables are not too strongly coupled with the vorticity and entropy characteristic variables.

There are discrepancies in the near field between the direct simulation and the solutions to the linearized Euler equations for the mixing layer to be presented. These discrepancies are probably due to hydrodynamic instabilities, but because the mixing layer is nonparallel (diverging), the instabilities do not grow without bound and they do not seriously affect the far-field solutions.

Approximations of Source Terms

One of the purposes of this work is to evaluate the effect of simplifications of the source terms in the linearized Euler equations. In the SNGR, only the velocities are modeled. This means that the source terms need to be simplified such that the fluctuations of temperature and density are zero. The first step in simplifying the source terms is to rewrite and approximate the heat source term in the energy equation. Begin by identifying

$$\rho h_0'' = \rho[(p/\rho) - (\bar{p}/\bar{\rho})][\gamma/(\gamma - 1)] + \tfrac{1}{2}\rho(u_k u_k - \widetilde{u_k u_k}) \qquad (28)$$

The first term can be written in terms of temperature. The first Reynolds term can be decomposed in Favre averages of velocities and the associated fluctuations. The last term can also be decomposed and rewritten in the same manner. After some algebra, the following expression is obtained:

$$\rho h_0'' = \rho C_p T'' + \rho\tilde{u}_k u_k'' + \tfrac{1}{2}\rho(u_k'' u_k'' - \widetilde{u_k'' u_k''}) \qquad (29)$$

which leads to

$$\rho h_0'' u_j'' = \rho C_p T'' u_j'' + \rho\tilde{u}_k u_k'' u_j'' + \tfrac{1}{2}\rho(u_k'' u_k'' - \widetilde{u_k'' u_k''})u_j'' \qquad (30)$$

If we neglect triple correlations of velocities, we obtain

$$\rho h_0'' u_j'' = \rho C_p T'' u_j'' + \rho\tilde{u}_k u_k'' u_j'' \qquad (31)$$

and, thus,

$$\rho h_0'' u_j'' - \overline{\rho h_0'' u_j''} = C_p(\rho T'' u_j'' - \overline{\rho T'' u_j''}) + \tilde{u}_k(\rho u_k'' u_j'' - \overline{\rho u_k'' u_j''}) \qquad (32)$$

The following notation is introduced:

$$\mathcal{T}_{ij} = \rho u_i'' u_j'' - \overline{\rho u_i'' u_j''}, \qquad \mathcal{Q}_j = C_p(\rho T'' u_j'' - \overline{\rho T'' u_j''}) \qquad (33)$$

Then the simplified source terms for the linearized Euler equations can be written as

$$\text{continuity} = 0, \qquad \text{momentum} = -\frac{\partial}{\partial x_j}(\mathcal{T}_{ij})$$

$$\text{energy} = -\frac{\partial}{\partial x_j}(\mathcal{Q}_j + \tilde{u}_i\mathcal{T}_{ij}) \qquad (34)$$

The next step in the simplification of the source terms is to neglect temperature fluctuations. The source terms are then

$$\text{continuity} = 0, \qquad \text{momentum} = -\frac{\partial}{\partial x_j}(\mathcal{T}_{ij})$$

$$\text{energy} = -\frac{\partial}{\partial x_j}(\tilde{u}_i\mathcal{T}_{ij}) \qquad (35)$$

In the last step of simplifications of the source terms fluctuations of density are neglected, that is,

$$\text{continuity} = 0, \qquad \text{momentum} = -\frac{\partial}{\partial x_j}\bar{\rho}(u_i'u_j' - \overline{u_i'u_j'})$$

$$\text{energy} = -\frac{\partial}{\partial x_j}\overline{u}_i\bar{\rho}(u_i'u_j' - \overline{u_i'u_j'}) \tag{36}$$

where the primed velocities now are fluctuations associated with the time-averaged velocities.

Numerical Simulation and Test of Source Terms

Numerical Scheme

The codes for the direct simulation and the linearized Euler equations are both based on conservative formulations using the same numerical scheme. The convective terms are discretized with a six-point stencil. The coefficients of Tam and Webb's[17] fourth-order dispersion-relation-preserving finite difference scheme are converted to the equivalent finite volume coefficients. The diffusive terms in the direct simulation code are discretized using a compact second-order scheme.[15] A fourth-order, four-step Runge–Kutta time-marching technique is used for the time stepping. Artificial selective damping is used to prevent spurious waves from the boundaries and regions with stretching to contaminate the solution.

The convective scheme is based on computing fluxes through the cell faces, and the artificial selective damping is added as follows. The conservative variables are computed on a cell face in a left-side and a right-side biased version using a high-order numerical scheme, and with use of a central second-order scheme, the eigenvalues associated with the characteristical variables are computed on the cell face. Depending on the sign of the eigenvalues, the corresponding characteristic variable is computed from the conservative variables on the cell face using the left- or right-side biased versions. The biasing of the conservative variables is introduced through the coefficients of the numerical scheme as

$$\begin{aligned} c_1 &= a_1 \pm \epsilon\ d_1 \\ c_2 &= a_2 \pm \epsilon\ d_2 \\ c_3 &= a_3 \pm \epsilon\ d_3 \\ c_4 &= a_4 \pm \epsilon\ d_4 \\ c_5 &= a_5 \pm \epsilon\ d_5 \\ c_6 &= a_6 \pm \epsilon\ d_6 \end{aligned} \tag{37}$$

where a_i are the coefficients of the symmetric convective scheme and d_i are chosen to approximate an odd-order derivative that is scaled with the small parameter ϵ of which the size is dependent of the order of the added derivative. The plus sign is used for the left-side bias and the minus sign for the right-side bias. Finally, the upwinded characteristic variables on the cell faces are transformed to physical variables and used to add the flux to the neighboring cells. In this way an even-order dissipative derivative is added to the calculation of the cell value. A more thorough description of the upwind biasing and the values of the coefficients are given in Refs. 14 and 15.

Boundary Conditions

The mixing layer consists of an upper stream with a Mach number of $M_1 = 0.5$ and a lower stream with Mach number $M_2 = 0.25$. At the interface between the two streams, a hyperbolic-tangent profile is used as inflow boundary profile. The mean inlet streamwise profile is

$$\tilde{u}_{\text{in}} = [(U_1 + U_2)/2] + [(U_1 - U_2)/2]\tanh[2y/\delta_\omega(0)] \tag{38}$$

where U_1 and U_2 are the upper and lower velocities, respectively. The initial vorticity thickness $\delta_\omega(0)$ defines the thickness of the incoming velocity profile (Fig. 1). The velocity at the inflection point is defined by $U_0 = (U_1 + U_2)/2$. The spanwise velocity $\tilde{v}_{\text{in}}$ is set to zero at the inlet. The pressure and density are constant over the inlet and are set to normal atmospheric conditions. The Reynolds number for this flow based on the initial vorticity thickness $\delta_\omega(0)$ is $Re_\omega = \delta_\omega(0)U_0/\nu = 1.58 \times 10^5$.

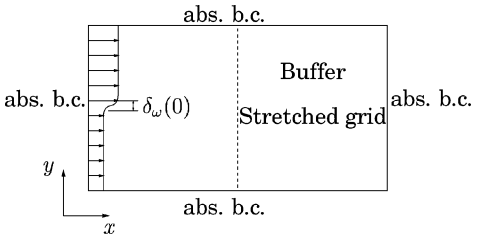

Fig. 1 Computational domain; absorbing boundary conditions used at all boundaries.

The absorbing boundary conditions used are based on local analysis of characteristic variables similar to the Thompson[18,19] boundary conditions, and the details are described in Refs. 14 and 20. The boundary conditions handle radiation (upper and lower) boundaries quite well as long as the outgoing waves to be absorbed are not at too high incidence angle and they are essentially nonreflecting for waves normal to the boundary. The amount of reflection from the radiation boundaries in this test case is very small, and the same holds for the inlet boundary. The reason for this is that the only disturbances reaching these boundaries are acoustic waves with comparably small amplitudes. At the outflow boundary, however, there are vorticity and entropy waves convected through the boundary, as well as acoustic waves. The large difference in energy of the vorticity and entropy waves leaving the computational domain at the outflow compared to the acoustic waves causes a major problem. Although most of the energy in the outgoing vorticity and entropy waves is absorbed and only a small portion of the energy is reflected back into the computational domain, the reflected part comes back as acoustic waves, contaminating the solution.

To aid the absorbing boundary conditions at the outflow region, a buffer region is applied at the last section of the computational domain. The mesh is also stretched in the flow direction in this region to help attenuate disturbances through the artificial dissipation in the numerical scheme. This method of taking care of outgoing disturbances was successfully used by Colonius et al.,[4] and Bogey et al.,[12] The term added to the governing equations is

$$\frac{\partial \boldsymbol{Q}}{\partial t} = \cdots - \frac{\bar{c}\sigma(x, y)}{\Delta x}(\boldsymbol{Q}') \tag{39}$$

where

$$\sigma(x, y) = \sigma_{\max}\left(\frac{x - x_0}{x_{\max} - x_0}\right)^2 \tag{40}$$

$\boldsymbol{Q}$ is the solution vector and $\sigma_{\max} = 0.1$; x_0 and $x_{\max}$ are the beginning and end of the buffer region. The disturbance $\boldsymbol{Q}'$ is in the direct simulation computed as $\boldsymbol{Q} - \bar{\boldsymbol{Q}}^*_{(n)}$. The term $\bar{\boldsymbol{Q}}^*_{(n)}$ is a time-average calculated using a low-pass filter, where the average at time step n is calculated from the average at time step $n-1$ and the solution at time step n as

$$\bar{\boldsymbol{Q}}^*_{(n)} = \alpha\bar{\boldsymbol{Q}}^*_{(n-1)} + (1 - \alpha)\boldsymbol{Q}_{(n)} \tag{41}$$

where α is a number close to one (further details later).

The parabolic shape of $\sigma(x, y)$ ensures that the damping term will minimize reflections back into the computational domain. The stretching of the mesh in the buffer region is also done gradually, with a very small amount of stretching at the beginning and more aggressive stretching once the damping term in the buffer region is larger. The same boundary conditions are used in the direct simulation as in the solution to the linearized Euler equations.

Forcing

A two-dimensional laminar shear layer is unstable by nature and will start to break up if the computational domain is long enough.

This process might take some time though, and the laminar part of the shear layer can be quite long in the streamwise direction. The acoustic field produced in this process also will be more or less stochastic with peaks in the spectra for the frequencies corresponding to the natural instability frequencies of the shear layer. To get better control of the shear layer and to make it break up faster, forcing is applied at the inflow boundary. This forcing is done using the inflow absorbing boundary conditions. The incoming vorticity characteristic variable is modulated at the fundamental frequency of the incoming profile. The resulting forcing enters the spanwise inflow velocity component as

$$v_{\text{in}} = \tilde{v}_{\text{in}} + A\sin(\omega_0 t) \tag{42}$$

where A is the amplitude of the forcing. The forcing is only applied in the region of the hyperbolic-tangent profile. Because the forcing is included as a part of the absorbing boundary conditions, the forcing does not interfere with the absorbing property of the boundary condition and the amount of spurious waves created by the forcing is kept to a minimum. An important detail is that the forcing added in the direct simulation is also added in the linearized Euler simulation. The reasoning behind this is that, unless this is done, the boundary condition for the linearized Euler simulation is not consistent with the sources evaluated from the direct simulation and disturbances not present in the direct simulation appear in the solution to the linearized Euler equations.

Bogey et al.[12] computed the fundamental instability frequency based on the instability theory of Michalke[21] as

$$f_0 = 0.132[U_0/\delta_\omega(0)] \tag{43}$$

The shear layer is forced at two frequencies, the fundamental frequency f_0 and half the fundamental frequency $f_0/2$. In this way, the forcing at the fundamental frequency will induce the creation of vortices that are convected downstream by the mean flow at a frequency of f_0. The second forcing at half the fundamental frequency will, in turn, induce a process where two successive vortices start to roll up around each other. This pair of vortices will, after a short period of time, start to merge and form a larger vortex. The frequency of this pairing will be denoted $f_p = f_0/2$ and the pairing time $T_p = 2T_0$. In this work, $A = 0.2$ for the forcing at the fundamental frequency f_0 and $A = 0.1$ for $f_0/2$.

Computational Setup

The computational mesh consists of 551×261 (x, y) mesh points. The physical size of the mesh is $0 \le x \le 6$ and $-3 \le y \le 3$, equivalent to $0 \le x \le 300\delta_\omega(0)$ and $-150\delta_\omega(0) \le y \le 150\delta_\omega(0)$ for $\delta_\omega(0) = 0.02$ m. The mesh is uniform in the streamwise direction for the first 451 points with a cell length of $\Delta x = 0.375\delta_\omega(0)$. The last 100 points are used to build the buffer region in which the mesh is stretched and damping terms are added to the equations. The last cell at the outflow boundary has a cell length of $\Delta x = 4.1\delta_\omega(0)$. In the spanwise direction, the mesh points are concentrated in the mixing region and stretched toward the outer boundary. The minimum cell height in the mixing region is $\Delta y = 0.164\delta_\omega(0)$ and increases slowly to $\Delta y = 0.3\delta_\omega(0)$ at $|y| \approx 5\delta_\omega(0)$. The stretching continues all of the way to the boundary, where the cell height is $\Delta y = 3.0\delta_\omega(0)$. With a fundamental frequency f_0 of 789 Hz the emitted sound waves have a wavelength of $\lambda = 0.87$ m, which corresponds to $14\Delta y$ in the outer region and so the propagating sound is well resolved in the entire domain.

Direct Simulation

The direct simulation started with the hyperbolic-tangent profile as an initial solution. To achieve a periodic solution, the simulation was run for 30,000 time steps at a Courant–Friedrichs–Lewy (CFL) number based on spectral radius[22] of CFL = 0.5, which is equivalent to 40 pairing periods T_p. During this time the low-pass filter average [Eq. (41)] was sampled with a value of the factor $\alpha = 0.9999$. This was done to ensure that the reference solution for the buffer layer would be representative of the true time average of the flow in the buffer layer. The sampling of the solution was then performed during 18,432 time steps. With a fixed time step at CFL ≈ 0.5, this is equivalent to 24 periods with 768 time steps per period.

In each time step, a limited part of the solution, called the source region, was saved. The source region was defined as $-20\delta_\omega(0) \le y \le 20\delta_\omega(0)$ and $0 \le x \le 300\delta_\omega(0)$. The total amount of disk space required for this simulation was about 30 GB.

Linearized Euler Equation Simulation

The linearized Euler simulation used the solution from the direct simulation as initial solution and was performed during 18,432 time steps. The time-averaged solution from the direct simulation was used as reference solution ($\bar{\rho}$, $\bar{\rho}\tilde{u}$, $\bar{\rho}\tilde{v}$, $\bar{\rho}\tilde{w}$, $\bar{\rho}\tilde{e}_0$), and at each time step, the solution from the direct simulation was used to evaluate the source terms. After the initial disturbances in the linearized Euler equations solution had left the computational domain, the solutions could be compared. This procedure was repeated with all four sets of source terms: the full source terms [Eq. (24)], the temperature-based terms [Eq. (34)], constant temperature terms [Eq. (35)], and constant density source terms [Eq. (36)].

Acoustic Solution

The far-field acoustic solution is displayed by the dilatation $\partial u_i/\partial x_i$. It is favorable to use dilatation as acoustic variable instead of pressure. The pressure in the direct simulation has a tendency to fluctuate in the computation at a very low frequency. The reason for this is probably associated with the absorbing boundary conditions, and this makes it hard to compare the pressure from the direct simulation with that from the linearized Euler solutions. The far-field dilatation is related to acoustic pressure as

$$\Theta = \frac{\partial u_i}{\partial x_i} = -\frac{1}{c_0^2\rho_0}\left(\frac{\partial p}{\partial t} + U_j\frac{\partial p}{\partial x_1}\right), \qquad j = [1, 2] \tag{44}$$

Given that the drift in pressure is linear in time, the dilatation will show a nonzero but constant time average. This seems to be confirmed with the results of the dilatation of the time-averaged solution, which show a nearly constant and nonzero dilatation in the far field. The dilatation of the direct simulation is, thus, instead compared to the dilatation of the fluctuations of the linearized Euler solutions. Vorticity is used to display the near field of the mixing layer.

Results

Figure 2 shows a snapshot of the vorticity in the near field and the dilatation in the far field for the direct simulation and the linearized Euler simulation with full source terms [Eq. (24)]. The solutions are very similar, and the phase and amplitude seem to agree well, although some wiggles that are visible in the direct simulation are

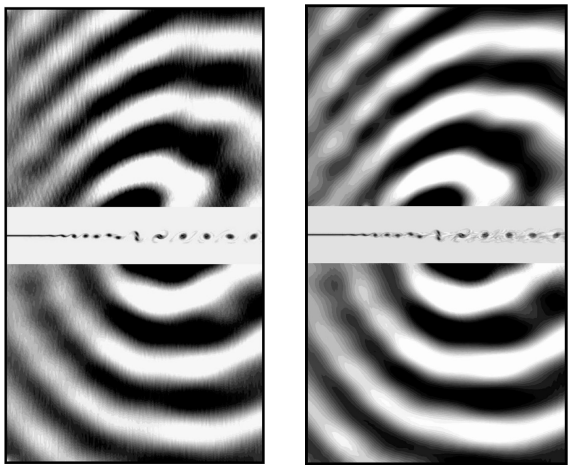

a) Direct simulation **b) Linearized Euler simulation with full source terms**

Fig. 2 Vorticity and dilatation for direct simulation and linearized Euler equations using the full source terms [Eq. (24)].

absent in the linear solution. The solutions from the linearized Euler simulations using the simplified sources [Eqs. (34–36)] are not shown because it is hard see any difference in the solutions compared to the simulation with full source terms.

Figure 3 shows the instant pressure fluctuation at $x = 2.0$ m and $0.5 \leq y \leq 3.0$ m for the direct simulation and the different linearized Euler solutions. The average pressure has been corrected for the direct simulation to avoid the problem with the drift in the average pressure. The phase and amplitude of the linearized Euler solutions are in good agreement with the direct simulation except very near the mixing layer. The solutions for the different source terms are clearly very similar.

Figure 4 shows a pairing of two vortices at four different stages. The time difference between Fig. 4a and Fig. 4d is equivalent to one-fourth of a pairing period. The pairing takes place at half the fundamental frequency and so the pairing period time is $T_p = 2T_0$. During this time, the merging vortices complete one-half rotation around each other. The vortex pair is a rotating quadrupole and as such has four lobes. Thus, the merging process results in one full period of sound emitted at a period time of T_p, that is, at the pairing frequency f_p of the mixing layer. The resulting wavelength of the emitted sound is $\lambda = c_0/f_p = 341.56/394.5 = 0.87$ m. It is during this time that most of the sound is generated and emitted.

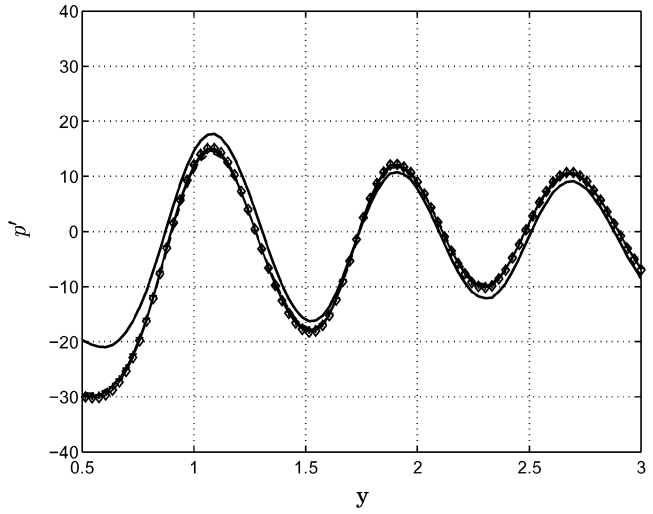

Fig. 3 Pressure disturbance at $x = 2.0$ m, $0.5 \leq y \leq 3$ m: solid line, direct simulation and other lines, different source terms.

There is a slightly biased directivity with two lobes in the lower and upper regions, and it is especially clear in the upper half of the computational domain. This double-lobe directivity was not observed in Ref. 12, but the computational configuration is not the same in this computation. Even if the reason for this double-lobe directivity could be of physical interest, this is not the major purpose of this study. To observe the same directivity in the direct simulation as in the linearized Euler equations simulation is the objective with this test.

Figure 5 shows the directivity of the time average of the square of the dilatation. Two lobes of directivity for the lower and upper regions are clearly marked at $\varphi \approx \{-95, -54, 39, 76 \text{ deg}\}$. This asymmetry in the directivity is a result of the different velocities in the upper and lower halves of the computational domain.

The linearized Euler equations with source terms clearly predict the effects of the inhomogeneous flowfield, and one can again see that there are very small differences in the solutions for the different source terms. Even when the source terms are based only on velocity fluctuations and all other unsteady effects are neglected, the solution was nearly exactly the same as for the full source terms. This implies that the major source of sound in this flow is fluctuations of vorticity. High-temperature effects have not been tested in this study and so the effects of simplifying the source terms for a high Mach number case or a high-temperature case is unknown. However, because the SNGR method is developed for simulations of the sound emitted from the turbulence in subsonic jets and not highly supersonic jets, these effects are outside the scope of this paper.

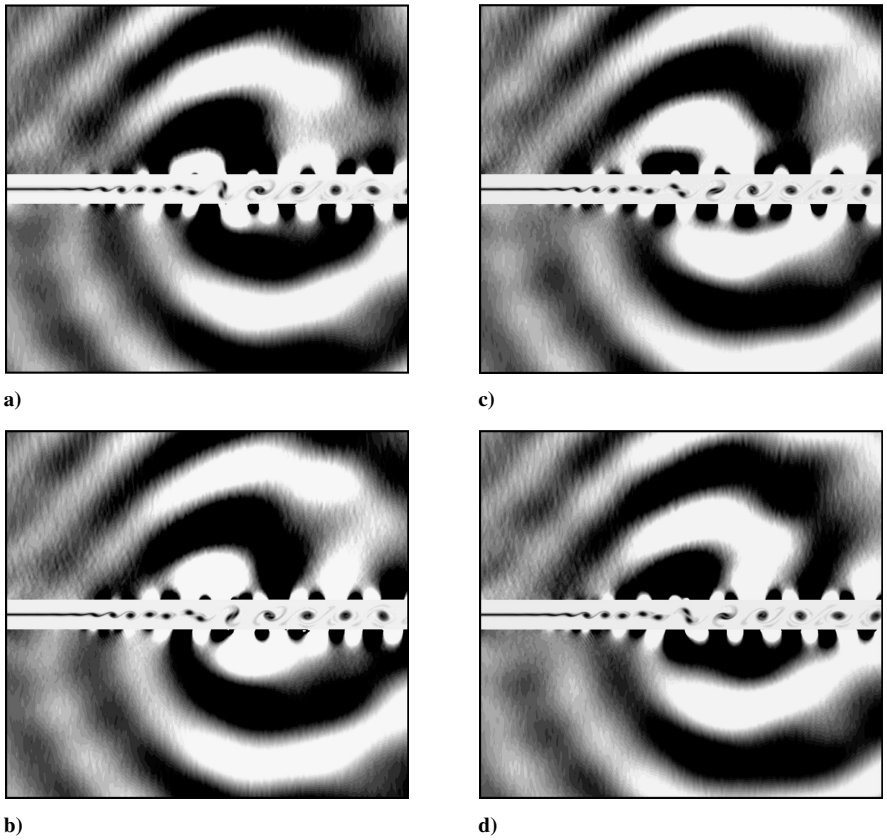

Fig. 4 Vorticity and dilatation for direct simulation: $0 \leq x \leq 3.26$ and $-1.5 \leq y \leq 1.5$.

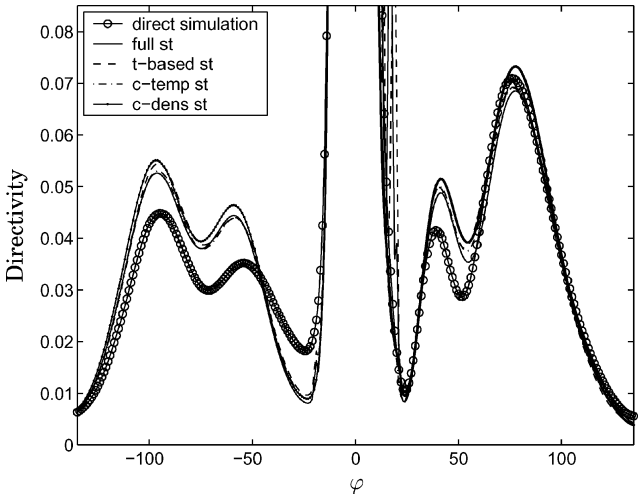

Fig. 5 Directivity as time average of square of dilatation at arc around $x_0 = 2.0, y_0 = 0$ with radius $r = 1.0$ at angles $-135 \leq \varphi \leq 0$ deg from the x axis and $x_0 = 1.6, y_0 = 0$ with radius $r = 1.0$ at angles $0 \leq \varphi \leq 135$ deg: direct simulation, full source terms, temperature based, constant temperature, and constant density.

Conclusions

Source terms for the linearized Euler equations in conservative form have been derived from the nonlinear Euler equations. The resulting inhomogeneous linearized Euler equations have been compared to two previous formulations of inhomogeneous linearized Euler equations, both in nonconservative formulations. The Goldstein formulation is found to be equivalent to the present formulation as an equation but not as an analogy because the source terms are not the same. The Bailly formulation is similar but not equivalent to the present formulation and the Goldstein formulation.

The conservative formulation of the linearized Euler equations with source terms is consistent with the conservative form of the Navier–Stokes equations, which minimizes the introduction of spurious waves. In this formulation it is also straightforward to introduce artificial selective damping through the numerical scheme.

Because the equations are to be used in the SNGR method, simplifications of the source terms have also been presented. These source terms have been tested through numerical simulations. The solutions from the direct simulation and the solutions from the proposed equations are in good agreement. Some differences are present, which are believed to be due to hydrodynamic instabilities and effects of the boundary conditions.

The solutions from using the different source terms are very similar. Even when the source terms are based only on velocity fluctuations and all other unsteady effects are neglected, the solution was nearly exactly the same as for the full source terms. This implies that the major sources of sound in this flow are fluctuations of vorticity.

These results show that an acoustic analogy based on the conservative form of the linearized Euler equations is a viable alternative to nonconservative forms presented previously. The conservative form has the advantage of maximum compatibility with the conservative form of the nonlinear flow equations.

References

[1]Lighthill, M., "On Sound Generated Aerodynamically, I. General Theory," *Proceedings of the Royal Society of London, Series A: Mathematical and Physical Sciences*, Vol. A 211, 1952, pp. 564–587.

[2]Lilley, G., "On the Noise from Jets," AGARD CP-131, 1974, pp. 13.1–13.12.

[3]Curle, J., "The Influence of Solid Boundaries upon Aerodynamic Sound," *Proceedings of the Royal Society of London, Series A: Mathematical and Physical Sciences*, Vol. A 231, 1955, pp. 505–514.

[4]Colonius, T., Lele, S., and Moin, P., "Sound Generation in a Mixing Layer," *Journal of Fluid Mechanics*, Vol. 330, 1997, pp. 375–409.

[5]Bechara, W., Bailly, C., Lafon, P., and Candel, S. M., "Stochastic Approach to Noise Modeling for Free Turbulent Flows," *AIAA Journal*, Vol. 32, No. 3, 1994, pp. 455–463.

[6]Bailly, C., Lafon, P., and Candel, S. M., "A Stochastic Approach to Compute Noise Generation and Radiation of Free Turbulent Flows," AIAA Paper 95-092, June 1995.

[7]Bailly, C., and Juvé, D., "A Stochastic Approach to Compute Subsonic Noise Using Linearized Euler's Equations," AIAA Paper 99-1872, May 1999.

[8]Billson, M., Eriksson, L.-E., and Davidson, L., "Jet Noise Prediction Using Stochastic Turbulence Modeling," AIAA Paper 2003-3282, May 2003.

[9]Billson, M., Eriksson, L.-E., Davidson, L., and Jordan, P., "Modeling of Synthetic Anisotropic Turbulence and Its Sound Emission," AIAA Paper 2004-2857, May 2004.

[10]Billson, M., Eriksson, L.-E., and Davidson, L., "Jet Noise Modeling Using Synthetic Anisotropic Turbulence," AIAA Paper 2004-3028, May 2004.

[11]Goldstein, M. E., "A Unified Approach to Some Recent Developments in Jet Noise Theory," *International Journal of Aeroacoustics*, Vol. 1, No. 1, 2002, pp. 1–16.

[12]Bogey, C., Bailly, C., and Juvé, D., "Numerical Simulation of Sound Generated by Vortex Pairing in a Mixing Layer," *AIAA Journal*, Vol. 38, No. 12, 2000, pp. 2210–2218.

[13]Bogey, C., Bailly, C., and Juvé, D., "Computation of Flow Noise Using Source Terms in Linearized Euler's Equations," *AIAA Journal*, Vol. 40, No. 2, 2002, pp. 235–243.

[14]Billson, M., "Computational Techniques for Turbulence Generated Noise," Ph.D. Dissertation, Div. of Thermo and Fluid Dynamics, Chalmers Univ. of Technology, Gothenburg, Sweden, May 2004.

[15]Eriksson, L.-E., "Development and Validation of Highly Modular Flow Solver Versions in G2DFLOW and G3DFLOW Series for Compressible Viscous Reacting Flow," Volvo Aero Corp., Internal Rept. 9970-1162, Trollhättan, Sweden, April 1995.

[16]Huerre, P., and Monkewitz, P. A., "Local and Global Instabilities in Spatially Developing Flows," *Annual Review of Fluid Mechanics*, Vol. 22, 1990, pp. 473–537.

[17]Tam, C., and Webb, J., "Dispersion-Relation-Preserving Finite Difference Schemes for Computational Acoustics," *Journal of Computational Physics*, Vol. 107, 1993, pp. 262–281.

[18]Thompson, K., "Time Dependent Boundary Conditions for Hyperbolic Systems, *I*," *Journal of Computational Physics*, Vol. 68, No. 1, 1987, pp. 1–24.

[19]Thompson, K., "Time Dependent Boundary Conditions for Hyperbolic Systems, *II*," *Journal of Computational Physics*, Vol. 89, No. 2, 1990, pp. 439–461.

[20]Eriksson, L.-E., "Lecture Notes, Compressible CFD," Div. of Thermo and Fluid Dynamics, Dept. of Mechanical Engineering, Chalmers Univ. of Technology, Gothenburg, Sweden, Oct. 2000.

[21]Michalke, A., "On the Inviscid Instability of the Hyperbolic-Tangent Velocity Profile," *Journal of Fluid Mechanics*, Vol. 19, 1964, pp. 543–556.

[22]Eriksson, L.-E., "Transfinite Mesh Generation and Computer-Aided Analysis of Mesh Effects," Ph.D. Dissertation, Dept. of Computer Sciences, Uppsala Univ., Uppsala, Sweden, March 1984.

H. Atassi
Associate Editor